An Analytical Model for Liquid and Gas Diffusion Layers in Electrolyzers and Fuel Cells

Rajora, A.; Haverkort, J.W.

DOI
10.1149/1945-7111/abe087

Publication date
2021

Document Version
Final published version

Published in
Journal of the Electrochemical Society

Journal of The Electrochemical Society

The Electrochemical Society
Advancing solid state & electrochemical science & technology

An Analytical Model for Liquid and Gas Diffusion Layers in Electrolyzers and Fuel Cells

Journal of The Electrochemical Society, 2021 **168** 034506

An Analytical Model for Liquid and Gas Diffusion Layers in Electrolyzers and Fuel Cells

A. Rajora[z] **and J. W. Haverkort**[z]

Process & Energy Department, Delft University of Technology, 2628 CB, Delft, the Netherlands

The diffusion layer is a crucial part of most fuel cells and electrolyzers. We analytically solve a simplified set of visco-capillary equations for the gas and liquid saturation profiles inside such layers. Contrary to existing numerical simulations, this approach allows us to obtain general scaling relations. We derive simple explicit equations for the limiting current density associated with reactant starvation, flooding, and membrane dehydration, including the effect of fluid properties, contact angle, tortuosity, and the pore size distribution. This is the first explicit, extensive and thorough analytical modeling framework for the two-phase transport in an electrochemical cell that provides useful insights into the performance characteristics of the diffusion layer. A more even pore size distribution generally allows higher currents. Explicit expressions for the minimum pore size and maximum layer thickness show that modern diffusion layers are typically well-designed.

 [DOI: 10.1149/1945-7111/abe087]

Manuscript submitted August 13, 2020; revised manuscript received January 6, 2021. Published March 4, 2021.

List of symbol

p	Pressure, [Pa]
p_c	Capillary pressure, [Pa]
p_t	Threshold pressure, [Pa]
u	Superficial velocity in x-direction, [m/s]
v	Interstitial velocity in x-direction, [m/s]
K	Absolute permeability, [m^2]
V	Molar volume, [m^3/mol]
j	Current density magnitude, [A/m^2]
$r_{\max}$	Maximum pore radius, [m]
R_c	Radius of curvature droplet/bubble [m]
c	Reactant concentration, [mol/m^3]
L	Thickness of the diffusion layer. [m]
D_0	Reactant diffusivity, [m^2/s]
D	Reactant diffusivity in porous medium, $D = D_0\epsilon^m$ [m^2/s]
D_{eff}	Effective diffusivity $\frac{D}{\int_0^1 s^{-n}d\bar{x}}$, [m^2/s]
T	Operating temperature, [K]
$j_\star$	Exchange current density, [A/m^2]
j_i	See Eq. 7 $j_i = J_i/\bar{L}$ [A/m^2]
b	Tafel slope, [V]
$j_{\max}$	Maximum j when $s_1 = s_{\min}$, [A/m^2]
$j_{\lim}$	Limiting j when $c_1 = 0$, [A/m^2]
$j_{\lim 0}$	Single phase $j_{\lim 0} = \frac{FDc_0}{z_w L}$ [A/m^2]
R	Gas constant 8.314 46, [J/mol/K]
F	Faraday constant 96 485.3329, [C/mol]
x	Coordinate across DL, [m]

Greek variables

μ	Dynamic viscosity, [Pa-s]
σ	Surface tension, [N/m]
τ	Tortuosity of the diffusion layer [-]
ρ	Density, [kg/m^3]
η	Activation overpotential, [V]
η_χ	Wetting overpotential, [V]
η_c	Concentration overpotential, [V]
α	Constant for DL in Eq. 8 [-]
λ	Pore size distribution index $p_c = p_t s^{-1/\lambda}$
ϵ	Porosity, [-]
χ	Wetted fractional surface area, [-]
Θ	Fractional bubble coverage, [-]
θ	Contact angle, [rad]

Subscripts and other notation

i	Phase index n or w
n	Non-wetting phase
w	Wetting phase
$*$	When $\frac{\bar{J}_n}{(1-s)^3} = \frac{\bar{J}_w}{s^3}$
0	Channel-DL interface, $\bar{x} = 0$
1	DL-CL interface, $\bar{x} = 1$
$\bar{A}$	Dimensionless quantity
~	Pertaining to catalyst layer
$'$	Derivative $d/d\bar{x}$
$-,+$	Left (-) or right (+) of interface
I_n^λ	$\equiv\int(1-s)^3 ds^{-1/\lambda}$
I_w^λ	$\equiv\int s^3 ds^{-1/\lambda}$

Dimensionless variables

$\bar{L}$	DL thickness $\bar{L} \equiv r_{\max}L/K$
$\bar{j}$	Current density j/j_i
m	Exponent in $D = D_0\epsilon^m$
n	Exponent in $D_{\text{eff}} = Ds^n$
k_i	Relative permeability
z_i	Stoichiometric coefficient
s	Saturation of the *wetting* phase
r	Order of the reaction
q	Exponent in $k_w = s^q$
$s_{\min}$	Minimum saturation

Increased awareness of greenhouse gases has prompted accelerated efforts for switching to renewable and cleaner sources of energy. Primary renewable energy sources like solar and wind have intermittent supply and hence require energy storage.[1] Hydrogen is an attractive energy carrier that can be obtained sustainably through electrolysis of water[2] and converted back to electricity using fuel cells.[3,4]

Fuel cells (FC) and water electrolyzers (WE) generally consists of a membrane electrode assembly (MEA) comprising a diffusion layer (DL), catalyst layer (CL), and a membrane, as shown in Fig. 1. The membrane is often a polymer electrolyte membrane (PEM) that transports cations, like protons, or an anion exchange membrane (AEM) that transports anions, like hydroxyl ions. The membrane serves to separate the reactants and the products formed at the two electrodes. The diffusion layer facilitates the transport of reactants

[z]E-mail: A.Rajora@tudelft.nl; J.W.Haverkort@tudelft.nl

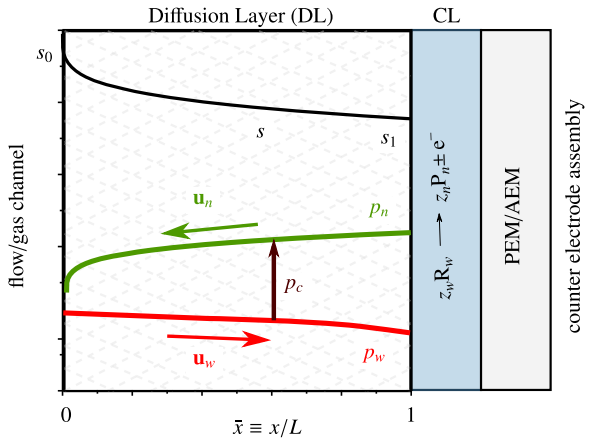

Figure 1. Illustrative profiles of s, p_n, and p_w throughout a diffusion layer. The wetting-phase saturation s is the volume fraction of the wetting phase reactant R_w relative to the total fluid volume. It runs between s_0 at $x = 0$ at the channel-DL interface and s_1 at $x = L$ at the DL-CL interface. The difference between the non-wetting phase pressure p_n and wetting phase pressure p_w is the capillary pressure p_c. The wetting and non-wetting phases moves with a superficial velocity $\mathbf{u}_w$ and $\mathbf{u}_n$ to the left and right, respectively. As a result the capillary pressure always increases and the saturation always decreases in the direction of $\bar{x}$.

and products to and from the catalyst layer. It provides an electrical connection between the catalyst layer and the current collector and provides the mechanical strength to allow high-pressure operation. Simultaneously, reaction products should be able to leave through the diffusion layer, while reactants move in the opposite direction to the catalyst layer. Therefore in the case of gaseous reactants and liquid products, as in a hydrogen fuel cell, for example, a *hydrophobic* gas diffusion layer (GDL) is used. The hydrophobicity makes the reactant gases the wetting phase, facilitating the transport of gases into the system. For the same reason, a *hydrophilic* diffusion layer is used in, for example, water electrolyzers, where water is the wetting phase. Reference 5 illustrates an exception where a hydrophobic layer is used to obtain bubble-free alkaline water electrolyzer operation, which requires water to be supplied from the opposite direction.

Figure 1 shows the transport of the wetting and non-wetting phases across the diffusion layer.

For PEM/AEM water electrolyzers and hydrogen fuel cells, the half-reactions in which liquid and gas phases move in opposite directions, are written as:

$$\textbf{PEM}:\ 2\,H_2O \underset{\text{Fuel Cell}}{\overset{\text{Electrolyzer}}{\rightleftarrows}} O_2 + 4\,H^+ + 4\,e^-,$$
$$\textbf{AEM}:\ 2\,H_2O + 2\,e^- \underset{\text{Fuel Cell}}{\overset{\text{Electrolyzer}}{\rightleftarrows}} H_2 + 2\,OH^-. \qquad [1]$$

In both fuel cells and water electrolyzers, water management is crucial. In water electrolyzers, water is the reactant and water starvation should be avoided.[6,7] Accumulation of oxygen in the anode catalyst layer is often held responsible for observed mass transport losses[8] although the origin is still very much under debate[9] and various, arguably less convincing hypotheses, have recently been proposed.[10,11]

In hydrogen fuel cells, too much product water can flood the diffusion layer, preventing the reactant gases from reaching the catalyst layer.[12] On the other hand, some water needs to be present to hydrate the membrane sufficiently for it to remain well conducting.

Various studies[13–17] provide models and insights, focusing on a single application. Here, the present model highlights the similarities in transport between different applications in which gases and liquids move in opposite directions. This is relevant for a wide range of applications including AEM/PEM hydrogen fuel cells,[18–20] water electrolyzers (WE),[21,22] direct alcohol fuel cells[23] like direct methanol fuel cells (DMFC)[24,25] and direct ethanol fuel cells (DEFC),[26,27] alkaline anion exchange membrane (AAEM) fuel cells,[28] and CO_2 gas diffusion electrodes (CO_2-GDE).[29–32]

Various researchers in the past have studied the two-phase flow in the diffusion layer of the electrochemical cells through numerical simulations.[13–17,19,33–35] and experiments[9,36–39] However, far fewer attempts have been made to establish analytical relations for limiting currents, effective diffusivity and saturation in a diffusion layer based on two-phase flow.[40,41] This work is an attempt to provide a new modeling perspective to the researchers in the electrochemical engineering community and provide explicit formulae that enable quick engineering estimates, can be used for analytical optimization, and in real-time energy management systems. By using these formulae, researchers can gain useful insight into the relevant parameters and their scalings.

The most important omission in this study is that the phase change between the gaseous and liquid phase due to condensation/evaporation in the diffusion layer is neglected. This means that the gas phase is assumed to be fully humidified so that the partial vapor pressure is equal to its saturation pressure, and the rate of phase change drops to zero. It should be noted that this assumption does not always hold, for example, in fuel cells operating at high temperature. In such cases, one needs to consider evaporation to represent the physical conditions more realistically. It has been shown that fully humidified conditions lead to poorer performance of fuel cells.[42] This means that the present model, neglecting the phase change, will underestimate the performance of the diffusion layer. It is also assumed that the water flux is linearly proportional to the current density. This requires that both the anode and the cathode are uniformly humidified, the pressure differential across the membrane is negligible and the back diffusion is limited.

We introduce the model equations and their approximate analytical solutions to define and provide expressions for the limiting current density and overpotentials associated with the diffusion layer. We validate our analytical model by comparing it with the experimental data given in Ref. 36, discuss its accuracy by comparing it with numerical solutions and, finally, summarize the key insights gained from the model.

Mathematical Model

Model equations.—Using a multiphase Darcy model[33,43–45] in 1-D, the pressure gradient of a phase i reads:

$$\frac{dp_i}{dx} = -\frac{\mu_i u_i}{K k_i}, \qquad [2]$$

where the *phase index* $i = w, n$ denotes either the wetting or non-wetting phase, u_i is the x-component of the *superficial velocity*, which can be both positive or negative, μ_i is the dynamic viscosity, k_i is the relative permeability, and K is the absolute permeability. Using Faraday's law

$$u_i = \pm\frac{z_i V_i}{F} j, \qquad [3]$$

with a plus sign for $i = w$ and a minus sign for $i = n$. Here j is magnitude of the total current density, V_i is the molar volume,[a] F is Faraday's constant, and z_i is the stoichiometric coefficient introduced in Fig. 1. Other sources of liquid flow proportional to the

[a] The appendix on the Stefan Velocity illustrates that V_i corresponds to the total molar volume, not the partial molar volume of the reaction or product species in case of mixtures. For an ideal gas, $V_i = RT/p_i$, where R is the gas constant, p_i is the partial pressure and T is the operating temperature.

current density j can be added to Eq. 3. For example, electro-osmotic drag of water through the membrane of a PEM can be approximately taken into account by adding $\frac{jV_n}{F}$ times the electro-osmotic drag coefficient, the average number of water molecules carrier per proton.

The capillary pressure is the pressure difference between the non-wetting and the wetting phase. Various models are proposed in the literature, like the Leverett-J function,[33,46] the van-Genuchten model,[47] the Brooks-Corey model[48] or analytical fractal models.[49,50] The Brooks-Corey relation[51–53] describes the capillary pressure as

$$p_c \equiv p_n - p_w = p_t s^{-1/\lambda}. \quad [4]$$

It is stressed here that *s is the saturation of the wetting phase*. For hydrophilic layers, s is the liquid saturation, while for hydrophobic layers, s is the gas saturation.

The threshold displacement pressure is related to the surface tension γ and contact angle θ by the Young-Laplace equation, that is valid for the capillary pressure when the pores would form cylindrical channels of radius $r_{\max}$, as

$$p_t = \frac{2\gamma|\cos(\theta)|}{r_{\max}}. \quad [5]$$

In a general porous medium, Eq. 5 may be interpreted as the definition of p_t, loosely related to the maximum pore size $r_{\max}$. A high value of the pore size distribution index λ is associated with a relatively flat capillary pressure curve, as illustrated in Fig. 2. This is associated with a more narrow pore size distribution, with most pores near the maximum pore size, and only a small fraction of smaller pores. Lower values of λ correspond to wider pore size distributions. It should be noted that the operating conditions in an electrochemical cell may also influence the $p_c - s$ curve through complex phenomena such as electrowetting. The Young-Lippmann equation[54–57] $\cos\theta = \cos\theta_0 + \frac{\varepsilon_0\varepsilon_r V^2}{2d\gamma}$ is often used to describe the dependence of contact angle on double layer thickness d and potential V. The variations in V are of the order jL/σ, with the effective electronic conductivity σ, and usually lead to only small variations in the contact angle.[58] Nevertheless, an applied potential can modify the contact angle from its value θ_0 in the absence of an applied potential, potentially resulting in undesirable phenomena.[30]

The relative permeabilities are often expressed as $k_w = s^q$ and $k_n = (1-s)^q$.[43] For the Brooks-Corey capillary pressure model, the relative permeabilities can be expressed as $k_w = s^{3+2/\lambda}$and$k_n = (1-s)^2(1-s^{1+\frac{2}{\lambda}})$.[59] Only in the limit $\lambda \gg 1$ do these reduce to the power law form with $q = 3$. The added complexity of using these more accurate expressions does not weigh up to the potential improvement in accuracy. Furthermore, different powers between 2 and 8 have also been used in the recent literature.[14] Therefore, in this work we will use the power law in its general form, but will also provide expressions for $q = 3$. Combining Eqs. 2 and 3 with Eq. 4, using $\bar{x} = x/L$, gives

$$\frac{ds^{-1/\lambda}}{d\bar{x}} = \frac{\bar{j}_n}{(1-s)^q} + \frac{\bar{j}_w}{s^q}, \quad [6]$$

where $\bar{j}_i = k_i|d(p_i/p_t)/d\bar{x}| = \mu_i|u_i|/p_t K$ is a dimensionless pressure gradient or velocity. With Eq. 3 it can also be interpreted as a dimensionless current density. Note that because the wetting phase moves in the positive x-direction and the non-wetting phase in the negative x-direction, both terms in Eq. 6 are positive, despite the minus sign in Eq. 4. With $\frac{ds^{-1/\lambda}}{d\bar{x}} = -\frac{1}{\lambda}s^{-\frac{1}{\lambda}-1}\frac{ds}{d\bar{x}}$, s is a monotonously decreasing function of $\bar{x}$. In Ref. 60 we study the complementary case of gas and liquid flowing in the same direction.

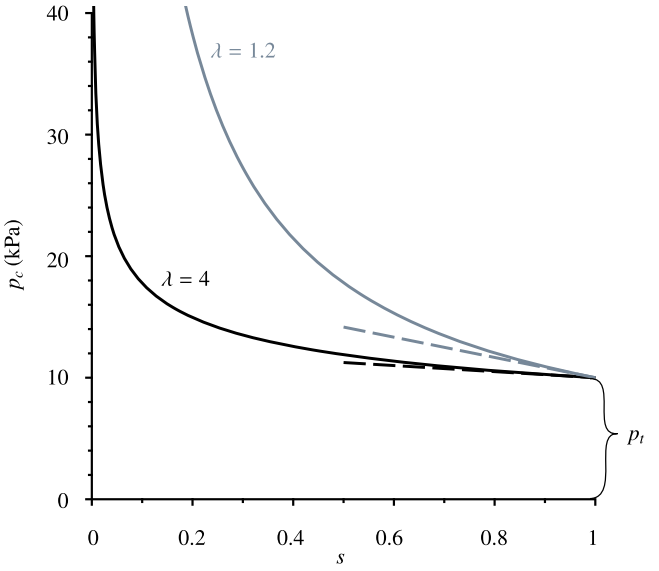

Figure 2. Capillary pressure curves for different pore size distribution index λ for $p_t = 10$ kPa. The dashed lines show the linearization $p_c = p_t\frac{1+\lambda-s}{\lambda}$ near $s = 1$ for the two different values of λ.

With Eqs. 2 and 3 we can write $\bar{j}_i = j/j_i$ where

$$j_i = \frac{p_t K}{\mu_i L}\frac{F}{z_i V_i} = \overbrace{\frac{2\gamma|\cos(\theta)|}{V_i}}^{j_i}\frac{F}{\mu_i z_i}\overbrace{\frac{1/\bar{L}}{\frac{K}{r_{\max}L}}}. \quad [7]$$

It should be noted that for applications like air fuel cells there will be consumption of oxygen at the catalyst layer, which has to be replenished. This can be done in part by diffusion but necessarily also at least in part by the so-called Stefan flow[61–63] as described in the appendix on the Stefan Velocity. In such cases, $\bar{j}_w$ will actually be lower than the one calculated using Eq. 3. As discussed below Eq. 3, additional transport of liquid through the membrane can be incorporated in j_i, as long as the associated flux is proportional to the current density. This is usually valid for high current densities, where the electro-osmotic flow dominates the transport through the membrane.[64,65] The expressions for saturation derived in the section on 21 can also be used for $\bar{j}_i$ varying non-linearly with current density j. For simplicity and providing insights, we will, however, continue to use the value of $\bar{j}_w$ given by Eq. 7.

Based on the work of Ref. 59, Refs. 66, 69 relate the permeability to the capillary pressure curve as $K = \alpha\epsilon^3\int_0^1 \frac{(\gamma\cos\theta)^2}{p_c^2}ds$, where the material-dependent constant α is of order unity. With Eq. 4 this gives[b]

$$K = \frac{\alpha\epsilon^3}{4}\frac{\lambda}{\lambda+2}r_{\max}^2. \quad [8]$$

This gives for $\bar{L} = r_{\max}L/K$

$$\bar{L} \equiv \frac{4(1+2/\lambda)}{\alpha\epsilon^3}\frac{L}{r_{\max}}. \quad [9]$$

so for a given porous material $\bar{L}$ is a multiple of the characteristic maximum pore size $r_{\max}$.

Boundary condition.—The relative permeability model of Eq. 2 assumes that there are continuous pathways for each phase. When

[b] Comparing with the Karman-Cozeny[68] result $K = \frac{d_p^2\epsilon^3}{180(1-\epsilon)^2}$, for a porous medium consisting of spherical particles of diameter d_p, this gives $r_{\max} = \frac{d_p}{1-\epsilon}\sqrt{\frac{1+2/\lambda}{45\alpha}}$.

applied to different porous media, the pressures across their interface are also assumed to be continuous. When bubbles or droplets are present at the flow channel-DL interface, they will typically be much larger than the maximum pore size so that their capillary pressure is much smaller than p_t. From Eq. 4, this implies that s remains close to its maximum, $s_0 \approx 1$.

As s_0 approaches unity, the interstitial velocity $v_n = u_n/\epsilon(1 - s_0)$ of the non-wetting phase starts to exert a non-negligible dynamic pressure $\frac{1}{2}\rho_n v_n^2$. With continuity of pressure, equating $\frac{1}{2}\rho_n v_n^2$ to p_t using Eq. 3 gives

$$s_0 \approx 1 - \sqrt{\frac{\rho_n}{2p_t}}\frac{z_n V_n}{\epsilon F} j. \qquad [10]$$

Even for very large current densities of many A cm^{-2} this usually negligibly deviates from $s_0 = 1$. Therefore, from now on, $s_0 = 1$ is used as a boundary condition. Recent measurements found this indeed to hold over a wide range of current densities in PEMWEs.[9] For PEMFCs something similar is found, although there the exact value of s_0 also depends on the relative humidity of the inlet gas and can be substantially different behind flow channel ribs.[69] High flow shear may invalidate this assumption of negligible bubble or droplet capillary pressure. Equation B·3 can be used to take this into account where we see a dependence of surface coverage and bubble curvature on the boundary condition s_0. Other authors have previously used a different constant value[33,70] or semi-empirical formula[71] as a boundary condition for s_0.

Note that we may modify Eq. 4 to $p_c = p_t(s^{-1/\lambda} - s_0^{-1/\lambda})$ without changing Eq. 6. In this case the maximum pore size disappears and for $s > s_0$ the capillary pressures becomes negative as in, for example, Ref. 72. Such a capillary pressure curve may roughly approximate a hydrophobic medium in which the largest pores are coated with a hydrophilic layer, or vice versa. Equal gas and liquid pressures at the channel-DL interface give $s = s_0$ as a boundary condition, as was also used in Ref. 19. Also, sometimes part of the saturation is considered immobile.[73] This fraction can, however, for most purposes be simply added to the solid volume fraction.

Analytical Solutions

Analytical solution for the saturation.—As discussed below Eq. 6, the wetting phase saturation s_1 at the DL-CL interface will be below that at the channel-DL interface, s_0. An exact analytical solution to Eq. 6 is not possible, so we approximate the solution by dividing the domain into two parts where we neglect either the first or the second term on the right-hand side, respectively. We define the saturation s_* as the saturation for which both terms are equal, which is the case when

$$s_* = \frac{1}{1 + (J_w/J_n)^{1/q}}. \qquad [11]$$

Note that in the presence of transport of species through the membrane, s_* may vary with current density, due to dependence of J_w/J_n on current density as discussed below Eqs. 3 and 7. The low power $1/q$, however, means that s_* will depend only weakly on current density.

For $s > s_*$ neglecting the second term on the right-hand side of Eq. 6 and integrating, gives

$$\bar{J}_n \bar{x} = I_n^\lambda|_{s_0}^s \quad (s > s_*). \qquad [12]$$

The integral $I_n^\lambda \equiv \int (1 - s)^q ds^{-1/\lambda} = -\frac{1}{\lambda}\int (1 - s)^q s^{-\frac{1}{\lambda}-1} ds$ can be performed analytically for integer q, so that

$$I_n^\lambda|_0^s = s^{-\frac{1}{\lambda}}\left(1 - \sum_{z=1}^{q}\frac{(-1)^z s^z}{z!(z\lambda - 1)}\prod_{k=0}^{z-1}(q - k)\right). \qquad [13]$$

For the values of λ where the denominator in one of the terms becomes 0, we can replace that term with $\frac{q!(-1)^{1/\lambda}\ln s}{(q - 1/\lambda)!(1/\lambda - 1)!}$. For $q = 3$, Eq. 13 gives

$$I_n^\lambda|_0^s = s^{\frac{-1}{\lambda}}\left(1 + \frac{3s}{\lambda - 1} - \frac{3s^2}{2\lambda - 1} + \frac{s^3}{3\lambda - 1}\right). \qquad [14]$$

Solving Eq. 12 for s in terms of $\bar{x}$ can only be done numerically. An approximation near $s \approx 1$ can however be obtained using the linearized capillary pressure shown in Fig. 2. Equation 6 with the second term neglected becomes

$$-\frac{1}{\lambda}\frac{ds}{d\bar{x}} = \frac{\bar{J}_n}{(1 - s)^q} \quad (s \approx 1), \qquad [15]$$

which is solved by $s \approx 1 - ((1 - s_0)^{1+q} + (1 + q)\lambda\bar{J}_n\bar{x})^{\frac{1}{1+q}}$, or with the boundary condition $s_0 = 1$

$$s \approx 1 - ((1 + q)\lambda\bar{J}_n\bar{x})^{\frac{1}{1+q}}. \qquad [16]$$

For $q = 3$, Eq. 16 gives

$$s \approx 1 - (4\lambda\bar{J}_n\bar{x})^{1/4} \quad (s \gtrsim 0.6). \qquad [17]$$

This analytical solution is similar to that obtained in Ref. 40 for a Leverett-J function capillary pressure relation. Comparing with the numerical solution for large λ shows that Eq. 17 is accurate to a relative error in $1 - s$ of at most 10 % when used for $s \gtrsim 0.6$. For lower values of $\lambda = 3$, 2, 1 rather only apply it for $s \gtrsim 0.65$, 0.7, 0.75, respectively.

When $s = s_*$ at $x = x_*$, Eq. 12 gives

$$\bar{x}_* = \frac{I_n^\lambda|_{s_0}^{s_*}}{\bar{J}_n} \underset{s_0 \approx 1}{\overset{s_* \gtrsim 0.6}{\longrightarrow}} \frac{(1 - s_*)^4}{4\lambda\bar{J}_n}. \qquad [18]$$

where the final expression was obtained from Eq. 17.

For $\bar{x} \geqslant \bar{x}_*$ the saturation drops below s_* and we will neglect the first term on the right-hand side of Eq. 6, so that integrating Eq. 6 gives

$$\bar{J}_w(\bar{x} - \bar{x}_*) = I_w^\lambda|_{s_*}^s \quad (s > s_*). \qquad [19]$$

The wetting integral $I_w^\lambda \equiv \int s^q ds^{-1/\lambda}$ evaluates to

$$I_w^\lambda|_0^s = -\frac{s^{q-\frac{1}{\lambda}}}{q\lambda - 1}, \qquad [20]$$

so that Eq. 19 gives

$$s = [s_*^{q-\frac{1}{\lambda}} - (q\lambda - 1)\bar{J}_w(\bar{x} - \bar{x}_*)]^{\frac{1}{q-1/\lambda}}. \qquad [21]$$

It should be noted that for a non-integer power q, the solution to Eq. 6 must be obtained numerically. In the subsequent analysis, we will use $q = 3$ while deriving expressions for limiting current and effective diffusivity to keep the equations clean and easy to understand. The analysis we provide henceforth, can also be extended to general q.

Analytical solution for the maximum current.—Various problems, like flooding in hydrogen fuel cells or membrane dehydration in water electrolyzers, are associated with a low saturation s_1. An important

question therefore is, what maximum current density is associated with a minimum saturation $s_{\min}$. The reasons for such a minimum saturation can be diverse, and may also depend on subjective criteria, an analysis of which is beyond the scope of this work.

When $s > s_*$, Eq. 12 immediately gives $j_{\max} = j_n I_n^{\lambda}|_{s_0}^{s_{\min}}$. Although useful and accurate when $s_{\min}$ is well above s_*, an arguably more insightful result is obtained when additionally $s_{\min} \gtrsim 0.6$ so that we may use the final expression in Eq. 17 to write

$$j_{\max} \approx \frac{j_n}{\lambda} \frac{(1 - s_{\min})^4}{4} \quad (s_{\min} \geqslant s_*). \qquad [22]$$

Inserting Eqs. 7 and 8 shows more clearly the dependence on the various parameters

$$j_{\max} \approx J_n \frac{\epsilon^3}{\lambda + 2} \frac{r_{\max}}{L} \frac{(1 - s_{\min})^4}{16}. \qquad [23]$$

where $J_n = 2\gamma|\cos(\theta)|\, F/V_n \mu_n z_n$ contains the non-wetting phase fluid properties. In terms of the diffusion layer properties, clearly a sufficient porosity ϵ and a pore aspect ratio $r_{\max}/L$ are beneficial for obtaining a high maximum current density while maintaining a sufficient saturation $s_{\min}$. The influence of the pore size distribution parameter is less strong and only shows a strong negative influence in case of very uniform pore size distributions with $\lambda \gg 1$.

When $s_{\min} < s_*$ we can solve Eq. 21 with $s = s_{\min}$ at $\bar{x} = 1$ for $\bar{j}_w = j/j_w$, to give

$$j_{\max} \approx \frac{j_w}{\lambda} \frac{s_*^{3-\frac{1}{\lambda}} - s_{\min}^{3-\frac{1}{\lambda}}}{(1 - \bar{x}_*)(3 - 1/\lambda)} \quad (s_{\min} \leqslant s_*). \qquad [24]$$

This is an implicit equation, since $\bar{x}_*$ depends on current density. If $s_* \gtrsim 0.6$, or from Eq. 11 $j_w \lesssim 0.3 j_n$, we can use the final expression in Eq. 18 to give[c]

$$j_{\max} \approx j_n \frac{(1 - s_*)^4}{4\lambda} + j_w \frac{s_*^{3-\frac{1}{\lambda}} - s_{\min}^{3-\frac{1}{\lambda}}}{3\lambda - 1} \quad (s_{\min} \leqslant s_*). \qquad [25]$$

Note that there may just as well be a maximum $s_{\max}$ to avoid, for example, membrane dehydration in case of a gas-fed fuel cell. In this case, the above equations can be used for a minimum current density $j_{\min}$, by interchanging the subscripts max and min.

Interpretation.—With $s_0 \approx 1$, the diverging first term on the right-hand side of Eq. 6 causes a rapid drop in saturation near the channel-DL interface as described by Eq. 17 and illustrated in Fig. 1. In this regime, Eq. 22 determines the maximum current density associated with a minimum saturation $s_{\min}$. The interpretation of this result is relatively straightforward. From Eq. 4 a driving capillary pressure gradient $dp_c/dx \approx -(p_t/\lambda)ds/dx$ is present near $s = 1$. This shows how a wider pore size distribution, associated with a lower value of λ, gives a higher driving capillary pressure gradient allowing a higher maximum current density. With $k_w = 1$, Eq. 15 would be solved by $s \approx 1 - \lambda \bar{j}_n$ so that $j_{\max} = j_n \frac{1 - s_{\min}}{\lambda}$. The wetting phase however strongly increases the friction through the relative permeability $(1 - s)^3$, which introduces the 4 in both the power and denominator of Eq. 22.

For $s \leqslant s_*$ the second term on the right-hand side of Eq. 6 dominates. This term represents the friction of the wetting phase, which in this regime determines the maximum current density. The presence of the non-wetting phase through the relative permeability s^3, in this case, introduces the $3 - 1/\lambda$ in Eq. 24. Once the wetting phase pressure gradient starts to dominate, the saturation has already decreased to s_*, but also the remaining distance $L - x_*$ to the catalyst layer, over which the capillary pressure gradient acts, has decreased, explaining the appearance of these terms in Eq. 24.

[c] For a general s_0, $(1 - s_*)^4$ is replaced by $(1 - s_*)^4 - (1 - s_0)^4$.

Finally, Eq. 25 combines the results of Eqs. 22 and 24. This may be interpreted in analogy with a series circuit of "resistances" proportional to $1/j_n$ and $1/j_w$, but also depending non-linearly on the "potential" s.

Note that, while in accordance with the discussion on the 12 we assumed a boundary condition $s_0 = 1$, it is straightforward to generalize the above equations to an arbitrary value of s_0. Also, note that when $s_0 \leqslant s_*$, we can use Eq. 21 with $s_* = s_0$ and $\bar{x}_* = 0$.

With a gaseous reactant and liquid product, usually $j_w/j_n = \mu_n z_n V_n/\mu_w z_w V_w \ll 1$ so that, from Eq. 11, $s_* \gtrsim 0.6$ and Eqs. 17, 22, and 25 can be used. Note that in this case, usually, the first term in Eq. 25 can be neglected.

Given the right integral I_n^{λ}, Eq. 12 can be used for any type of capillary pressure relation. Even different relative permeability models can be accommodated after suitably re-defining s_*. In the appendix on the Udell Leverett-J Function we work out the integral I_n^{λ} for the Leverett-J function.

Performance Losses in a Diffusion Layer

Activation overpotentials η.—A limiting current density arises when reactants cannot diffuse to the catalyst layer at a sufficient rate. We assume that the concentration-dependent Tafel equation describes the half-reaction in the catalyst layer as:

$$j = \chi j_\star \left(\frac{c_1}{c_0}\right)^r \exp\frac{\eta}{b}, \qquad [26]$$

where r is the order of the reaction in the reactant concentration c_1, assumed constant throughout the thin catalyst layer, χ is the fraction of total surface area covered by the wetting phase reactant, $j_\star$ is the superficial exchange current density of the catalyst layer[74] at the bulk concentration c_0 at $\bar{x} = 0$, and the Tafel slope b. Rearranging Eq. 26, the activation overpotential η is split into three separate terms

$$\eta = \overbrace{b \ln \frac{j}{j_\star}}^{\eta_a} + \overbrace{b \ln \frac{1}{\chi}}^{\eta_\chi} + \overbrace{rb \ln \frac{c_0}{c_1}}^{\eta_c}. \qquad [27]$$

Here η_a is the overpotential required when the entire reactive area is wetted with reactant at the concentration c_0. In Eq. 27 η_χ is the additional overpotential due to the non-wetting phase covering a fraction χ of the reactive area, and η_c is the concentration overpotential.

Note that, an often considered voltage loss that is not mentioned in Eq. 27 is the change in equilibrium potential due to the dissolved gases.[6,7,11,17,71,76,77] If the associated reaction steps are not rate-determining, they may be considered in equilibrium and described by the Nernst equation

$$\Delta E_{\text{mt}} = \frac{RTz_n}{F} \ln \frac{C}{C_{\text{ref}}}, \qquad [28]$$

with C the concentration of the dissolved product gases at the position of the catalyst layer, and C_{ref} a reference value. See, for example, Ref. 11 for a simple model to estimate C.

Wetting overpotential η_χ.—Using the Brooks-Corey $p_c - s$ curve, the volumetric surface area a_w of the catalyst layer covered by the wetting phase[78] can be written as:

$$a_w = \frac{2\epsilon}{r_{\max}} \int_0^{\tilde{s}} \tilde{s}^{-\frac{1}{\tilde{\lambda}}} d\tilde{s} = \frac{2\epsilon}{r_{\max}} \frac{\tilde{\lambda}}{\tilde{\lambda} - 1} \tilde{s}^{\frac{\tilde{\lambda}-1}{\tilde{\lambda}}}, \qquad [29]$$

Variables dressed with a *tilde* denote the properties of the catalyst layer. It should be noted that Eq. 29 is only valid for $\tilde{\lambda} > 1$. For $\tilde{\lambda} \leqslant 1$, the integral diverges unless we define a minimum saturation. The reason is that for such a wide pore size distribution the smallest pores have an infinite surface area. When $s = 1$, Eq. 29 gives

$a_{w,\max} = \frac{2\epsilon}{r_{\max}}\frac{\tilde{\lambda}}{\tilde{\lambda}-1}$, while at a saturation s the relative surface area covered by the wetting phase is given by

$$\eta_\chi = \frac{a_w}{a_{w,\max}} = (1/\tilde{\lambda} - 1)b \ln \tilde{s}. \quad [30]$$

As the catalyst layer pore size distribution parameter $\tilde{\lambda} \to 1$, Eq. 30 gives that $\eta_\chi \to 0$ and the surface coverage does not adversely impact performance. The reason is that the smallest pores, that have most of the surface area, remain available for the reaction. If $\tilde{\lambda} \gg 1$, Eq. 30 reduces to $\eta_\chi = -b \ln \tilde{s}$, which is used, for example, in Refs. 70, 71. In liquid-phase electrolyzers this is often referred to as the bubble overpotential.[7]

For a very thin catalyst layer formed by spraying small particles on the diffusion layer, we may use $\tilde{s} = s_1$. For a more extended layer, with potentially a wettability different from that of the diffusion layer, continuity of the capillary pressure[79,80] is assumed which, from Eq. 4, gives $\tilde{s} = (p_t s_1^{-1/\lambda}/\tilde{p}_t)^{-\tilde{\lambda}}$. Both of these models are, however, obviously simplifications that have to be used with caution. The latter formula for example, may give rise to $\tilde{s} > 1$ in case of very small catalyst layer pores, something that may be ameliorated by including dynamic pressures as in the Appendix on the boundary condition for s1. Often there will be a mixed wettability in the catalyst layer, influencing the relation between s_1 and $\tilde{s}$.

Concentration overpotential η_c**.—**In water electrolyzers, water is present in high concentrations ($c_1 \approx c_0$) and any transport losses occur mainly due to the surface area of the catalyst layer getting covered by gas. For applications such as hydrogen fuel cells or CO_2-reduction-GDEs, reactant gases have to diffuse through either a mixture of gases or through water to reach the catalyst surface.[35] In the dilute limit, c_1 can then be obtained from Fick's law[34,81] for the molar flux

$$\frac{z_w}{F} j = D_{\text{eff}} \frac{c_0 - c_1}{L}, \quad [31]$$

where D_{eff} is the effective diffusion coefficient, modified by the saturation profile. A limiting current is obtained when $c_1 \to 0$, which gives

$$j_{\lim} = \frac{F D_{\text{eff}} c_0}{z_w L}. \quad [32]$$

In the absence of the non-wetting phase, a limiting current density is given by

$$j_{\lim 0} = \frac{F D c_0}{z_w L}, \quad [33]$$

where $D = D_0\epsilon/\tau$ in terms of the porosity ϵ and tortuosity τ, and the single phase diffusivity D_0. Often a power law relation $\tau = \epsilon^{1-m}$ approximately holds so that $D = D_0\epsilon^m$. It has been pointed out that $m = 1.5$ as in Bruggeman's correlation underestimates the effect of tortuosity in diffusion layers and often a value between 2 and 5 is more appropriate.[82,83]

Inserting c_1 from Eq. 31 in η_c from Eq. 27 gives the concentration overpotential as

$$\eta_c = rb \ln\left(\frac{1}{1 - j/j_{\lim}}\right). \quad [34]$$

Effective diffusivity D_{eff}**.—**The diffusivity of gases in liquids is several orders of magnitude lower than that in the gases, so we may neglect the transport of gases in the liquid phase. This implies that the transport of reactant gas in the presence of liquids will be less effective than in a dry GDL so that the limiting current is also lower. We can approximately incorporate this by the replacing the diffusivity with Ds^n.[84] In the presence of a liquid non-wetting phase, neglecting the diffusion of gas through the liquid, Fick's law in the dilute limit, can therefore, be written as

$$\frac{z_w j}{F} = D s^n \frac{dc}{dx}. \quad [35]$$

In general, the exponent n can differ from the exponent m, but is also typically in the range between 2 and 5.[82,83] Using Eqs. 31 and 35, the effective diffusivity of the gaseous wetting phase can be written as:

$$\frac{D}{D_{\text{eff}}} = \int_0^1 s^{-n} d\bar{x}. \quad [36]$$

For a high-s design GDL $s \geqslant s_* \gtrsim 0.6$. When, furthermore $s_0 \approx 1$, Eqs. 17 and 36 give

$$\frac{D}{D_{\text{eff}}} \approx \int_0^1 (1 - (4\lambda\bar{J}_n \bar{x})^{1/4})^{-n} d\bar{x}, \quad [37]$$

To first order in $(4\lambda\bar{J}_n\bar{x})^{1/4}$ the integrand reads $1 + n(4\lambda\bar{J}_n\bar{x})^{1/4}$. Performing the integrating therefore gives to leading order $1 + \frac{4n}{5}(4\lambda\bar{J}_n)^{1/4} \approx \left(1 - \frac{4n}{5}(4\lambda\bar{J}_n)^{1/4}\right)^{-n}$. The second expression turns out to be a substantially more accurate approximation, with which Eq. 37 becomes

$$\frac{D}{D_{\text{eff}}} \approx \left(1 - \frac{4}{5}(4\lambda\bar{J}_n)^{1/4}\right)^{-n}. \quad [38]$$

For a low-s design GDL, we consider that $s < s_\star$. Using the same approach as for the 21, the integral in Eq. 36 is split in two parts to give

$$\frac{D}{D_{\text{eff}}} = \int_0^{\bar{x}_*} s^{-n} d\bar{x} + \int_{\bar{x}_*}^1 s^{-n} d\bar{x}. \quad [39]$$

Inserting Eq. 6 in Eq. 39 and neglecting the wetting phase pressure gradient for $\bar{x} < \bar{x}_*$ and the non-wetting phase pressure gradient for $\bar{x} > \bar{x}_*$, we can integrate by changing variables to give

$$\begin{aligned}\frac{D}{D_{\text{eff}}} &= \int_{s_0}^{s_*} \frac{-s^{-\frac{1}{\lambda}-m-1}(1-s)^3}{\lambda\bar{J}_n} ds + \int_{s_*}^{s_1} \frac{-s^{2-\frac{1}{\lambda}-m}}{\lambda\bar{J}_w} ds \\ &= \frac{\lambda_n}{\lambda}\left(\frac{\int_{s_0}^{s_*}(1-s)^3 ds^{-\frac{1}{\lambda_n}}}{\bar{J}_n} + \frac{\int_{s_*}^{s_1} ds^{3-\frac{1}{\lambda_n}}}{\bar{J}_w(1-3\lambda_n)}\right),\end{aligned} \quad [40]$$

where $\lambda_n = \frac{\lambda}{1+\lambda n}$. These integrals are those of Eqs. 12 and 20 with λ_n instead of λ. Therefore we can rewrite Eq. 40 as

$$\frac{D}{D_{\text{eff}}} \approx \begin{cases} \frac{\lambda_n}{\lambda}\frac{I_n^{\lambda_n}|_{s_0}^{s_1}}{\bar{J}_n} & s_1 > s_* \\ \frac{\lambda_n}{\lambda}\left(\frac{I_n^{\lambda_n}|_{s_0}^{s_*}}{\bar{J}_n} + \frac{I_w^{\lambda_n}|_{s_*}^{s_1}}{\bar{J}_w}\right) & s_1 \leqslant s_*. \end{cases} \quad [41]$$

We hope that no confusion arises because of our use of a subscript n here, not referring to the non-wetting phase but instead to the exponent n in Eq. 36. The quantity in Eq. 41, inversely proportional to the effective diffusivity, is a dimensionless mass transfer resistance and has the structure of two resistances in series.[d]

[d] Note that for $\lambda = \lambda_n$, using Eqs. 18 and 19, the first and last term between brackets of Eq. 41 become $\bar{x}_*$ and $1 - \bar{x}_*$ so that $D_{\text{eff}} = D$ as it should for $n = 0$.

Diffusion limited current density $j_{\lim}$.—First we consider the case in which $s_1 \geqslant s_* \gtrsim 0.6$ so that with $s_0 \approx 1$, Eq. 17 can be used. In this case we can derive the Eq. 38, or with $4(4/5)^4 \approx 1.6$

$$\frac{D}{D_{\text{eff}}} \approx \left(1 - \left(1.6\lambda \frac{j}{j_n}\right)^{1/4}\right)^{-n}. \quad [42]$$

From Eq. 17 this remains valid up to $1.6\lambda\frac{j}{j_n} \approx 0.01$ in which case the diffusivity is reduced by a factor 0.68^n. This exponential dependence on n highlights the importance of straight non-tortuous gas pathways, potentially using techniques as in Ref. 85, that lower n. Inserting into Eq. 32 gives

$$j_{\lim} \approx j_{\lim 0}\left(1 - \left(1.6\lambda \frac{j_{\lim}}{j_n}\right)^{1/4}\right)^{n}. \quad [43]$$

Comparing with the numerical solution for $\lambda \geqslant 1$ shows that this approximation has a relative error below 10% when $j_{\lim} \lesssim j_n \frac{0.003}{n+\lambda}$. In general, this implicit equation has to be solved numerically. When, however, $n = 4$ we find

$$j_{\lim} \approx \left(j_{\lim 0}^{-1/4} + \left(\frac{j_n}{1.6\lambda}\right)^{-1/4}\right)^{-4}. \quad [44]$$

Note that $j_{\lim}$ will always be lower than the smallest of $j_{\lim 0}$ and $j_n/1.6\lambda$. This makes sense, as the presence of the non-wetting phase can only lower the effective diffusivity and therewith the diffusional limiting current.

Next, we consider the case in which $s_1 < s_*$ for which the bottom result of Eq. 41 has to be used. Inserting into Eq. 32 gives an implicit equation

$$I_n^{\lambda_n}|_{s_0}^{s_*} j_n + I_w^{\lambda_n}|_{s_*}^{s_1} j_w \approx j_{\lim 0}(1 + \lambda n). \quad [45]$$

When the first term can be neglected[e] this gives, after some algebra

$$j_{\lim} \approx j_w s_*^{3-\frac{1}{\lambda}} \frac{1 - \left(1 + \frac{j_{\lim 0}}{j_w}\frac{1-\lambda(3-n)}{s_*^{3-1/\lambda_n}}\right)^{\frac{3-1/\lambda}{3-1/\lambda_n}}}{(3\lambda - 1)(1 - x_*)}, \quad [46]$$

where s_* and x_* are given by Eqs. 11 and 11, respectively. Equation 46 simplifies in the following two limits

$$j_{\lim} \approx \begin{cases} \dfrac{j_w}{1-\bar{x}_*}\dfrac{s_*^{3-\frac{1}{\lambda}}}{3\lambda - 1} & \dfrac{j_{\lim 0}}{j_w s_*^{3-1/\lambda_n}} \gg 1 \\ \dfrac{j_{\lim 0} s_*^m}{1-\bar{x}_*} & \dfrac{j_{\lim 0}}{j_w s_*^{3-1/\lambda_n}} \ll 1. \end{cases} \quad [47]$$

The above equation is exactly Eq. 25 for $s_{\min} = 0$, which makes sense since when the saturation s_1 vanishes, the effective diffusivity vanishes as well, causing a limiting current. If $s_* \gtrsim 0.6$ we can use Eq. 18, similar to in Eq. 25, to give for the bottom case of Eq. 47

$$j_{\lim} \approx j_{\lim 0} s_*^n + j_n \frac{(1 - s_*)^4}{4\lambda}. \quad [48]$$

Here $j_{\lim 0}$ is reduced by a factor s_*^n due to the lower saturation s_*, which in this limit does not drop much further. The final term in Eq. 48 adds a bit for the initial part where $s > s_*$.

[e] When $s_* \gtrsim 0.6$ we can use Eqs. 18, 20, 11 to write $\frac{1-s_*}{4\lambda_n} \ll \frac{s_*^{3-\frac{1}{\lambda_n}} - s_1^{3-\frac{1}{\lambda_n}}}{s_*^3(3\lambda_n - 1)}$. This is usually the case when s_1 drops somewhat below s_*, or from Eq. 18 when $j \gtrsim j_n \frac{(1-s_*)^4}{4\lambda}$.

Results and Discussion

For the hydrophobic SGL carbon paper, Toray090, E-Tek Cloth "A" and Lyflex felts, λ lies between 0.95-4 and p_t varies between 6–39 kPa.[86] These hydrophobic diffusion layers are typically a few hundred micrometres thick.[86,87] Water electrolyzers usually have titanium-based hydrophilic layers with the largest pore diameter roughly 12–16 μm, the permeability of the order 10^{-12} m^2, and a thickness around 1 mm[88] corresponding to a threshold pressure p_t of the order of 10 kPa. For illustration, we choose the diffusion layer parameters for both electrolyzers and fuel cells to be same as that of Toray090[86] for which $\lambda \approx 4$ and $p_t = 10$ kPa. Table I lists the properties for exemplary gaseous and liquid wetting phase cases, representative of a typical PEM fuel cell and water electrolyzer, respectively.

Numerical verification of the analytical model.—Figure 3a shows a comparison between analytical and numerical saturation profiles for the two cases listed in Table I. The analytical solution for the wetting phase saturation is always higher than the numerical solution. This is expected, because we always neglect one of the terms on the right-hand side of Eq. 6 and hence underestimate the capillary pressure gradient. The agreement with Eq. 17 is nonetheless good since s remains rather high.

In Fig. 3b we also show a case where we increased $\bar{L}$ to show the effect of, for example, a much smaller pore size. In this case in part of the diffusion layer the wetting phase pressure gradient dominates, represented by the final term in Eq. 6. In this case we used the analytical result of Eq. 21 for which the agreement with the numerical result is reasonable.

Experimental validation of the analytical model.—We validate our analytical model by comparing the saturation profile across the SGL10 BB diffusion layer of a PEM fuel cell with the experimental data obtained in Ref. 36 from high resolution neutron radiography. The SGL10 BB diffusion layer consists of both a gas diffusion layer (GDL) and microporous layer (MPL). The diffusion layer properties are listed in Table II. The liquid thickness is defined as the integral amount of liquid encountered by a neutron beam in the direction perpendicular to the flow in the diffusion layer. The liquid saturation, $1 - s$, obtained from our model is converted into corresponding liquid thickness using the following equation

$$t = t_0(1 - s)\epsilon, \quad [49]$$

where t_0 is the width of the diffusion layer. The width of the diffusion layer t_0 in the experiments was 6 mm. The liquid thickness in the membrane is taken to be equal to 1.6 mm as given in the same experimental reference.[36] Due to the finite resolution of the neutron radiography in the experiments and high water content in the membrane, the liquid content in the MPL appears to be much higher in the neutron radiographs than it actually is Ref. 36. To take this instrumental broadening into account and allow a direct comparison to the neutron radiographs, the neutron detector point spread function is used to perform 1-D convolution on our analytical results. The details of the neutron point detector function can be found in Ref. 36.

Figure 4 shows a comparison of experimental results and model prediction using Eq. 17 for a current density of 300 mA cm^{-2} at 80 °C and the properties of the diffusion layer listed in Table II. Due to the low current density in the experiments, the effects of evaporation can be neglected. We see that the agreement between the analytical predictions and experimental results is good. The small quantitative disagreements may be attributed to the fact that the properties of the diffusion layer are assumed to be constant in our model, while in reality, these properties may vary across the diffusion layer. Calculating the properties of the compressed layer from the properties of the uncompressed layer may also contribute to the quantitative error. This highlights the importance of benchmarking the

Table I. Characteristics and operating conditions for example diffusion layers at 1.2 bar and 60 °C. The common structural parameters used are $K = 8 \cdot 10^{-12}$ m^2, $p_t = 10$ kPa, $r_{\max} = 10$ μm, $2\gamma|\cos\theta| = 0.1$ N/m, $\lambda = 4$, $m = n = 3$, and $\epsilon = 0.78$.[86] A diffusivity $D_{O_2} = 2 \cdot 10^{-5}$ m^2 s^{-1} for oxygen in air gives $j_{\lim 0} = 11$ A cm^{-2}. Note that for μ_n and V_n property we used the wetting phase properties of the adjacent column.

Wetting phase	Gaseous	Liquid
Examples	PEMFC, AEMFC, CO_2-GDE	PEMWE, AEMWE, Direct alcohol fuel cells
L [μm]	300 [86]	1000 [88]
$\bar{L} = r_{\max} L/K$	375	1250
μ_w [Pa-s]	$2.2 \cdot 10^{-5}$	$4.7 \cdot 10^{-4}$
V_w [m^3/mol]	$23 \cdot 10^{-3}$	$1.8 \cdot 10^{-5}$
$1/z_w$	4	2
$1/z_n$	2	4
s_*	0.75	0.25
J_w/J_n	0.03	30
J_w [A/m^2]	$7.6 \cdot 10^{10}$	$2.3 \cdot 10^{12}$
J_n [A/m^2]	$2.3 \cdot 10^{12}$	$7.6 \cdot 10^{10}$
j_w [A/m^2]	$2 \cdot 10^{8}$	$1.8 \cdot 10^{9}$
j_n [A/m^2]	$6.1 \cdot 10^{9}$	$6.1 \cdot 10^{7}$
j [A/m^2]	$2 \cdot 10^{4}$	$2 \cdot 10^{4}$

Table II. Properties of an SGL10BB diffusion layer used in Fig. 4. In Ref. 36, the diffusion layer is compressed from the original thickness $L_0 = 420$ μm to the compressed thickness, $L = 254$ μm. To calculate the compressed porosity, it is assumed that the solid material in the diffusion layer is incompressible.[89] The Brooks-Corey parameters for the MPL are calculated from the van-Genuchten parameters in Ref. 86 using relations given in Ref. 90.

Property	GDL	MPL
Compressed Thickness [μm]	188	62
Porosity	0.84 [86]	0.72 [86]
Compressed Porosity	0.73	0.53
p_t [bar]	0.06 [86]	8.75
λ	1.61 [86]	0.86
K [m^2]	$3.74 \cdot 10^{-11}$ [91]	$5.3 \cdot 10^{-13}$ [91]

diffusion layer properties at different compression conditions. Nevertheless, the analytical model shows a good agreement with the experimental data presented in Ref. 36.

Maximum current density.—For the properties listed in Table I, to reach $s_{\min} = 0$, according to Eq. 24 requires a current density $j_{\max} \approx 10^7$ A/m^2 for both layers. This extremely high current density shows that for the typical diffusion layer properties of Table I there will be no risk of approaching $s_{\min} = 0$.

Although the boundary condition $s_0 \approx 1$ was argued to be the relevant boundary condition for most cases, in Fig. 5 we show the effect of s_0 on the $j_{\max}$. This can be useful for mixed-wettability layers and because different boundary conditions are sometimes used.[19,70,71] Figure 5 shows that the maximum current $j_{\max}$ is insensitive to the exact boundary condition when s_0 is close to 1. The reason is the large drop in s that occurs in a very thin layer near $\bar{x} = 0$ seen in Fig. 3. This strong decrease is caused by the first term on the right-hand side of Eq. 6 and described by the formula given just above Eq. 17.

Limiting current density.—Air with 21 v% of oxygen at 1.2 bar and 60 °C has an oxygen concentration of $c_0 = 9.1$ mol/m^3,[f] so that with $D_{O_2} = 2.10^{-5}$ m^2 s^{-1}, $n = 3$, and the gaseous wetting phase properties in Table I, we find a single phase diffusion-limited current density of $j_{\lim 0} = FDc_0/z_w L \approx 11$ A cm^{-2}. Since this is below $0.01 j_w/4\lambda$ we can use Eq. 42 to calculate D_{eff}. Solving Eq. 32 for $j = j_{\lim}$ iteratively gives $j_{\lim} \approx 8.1$ A cm^{-2}. The presence of water in this case actually only moderately decreases the limiting current density, which is expected giving the high saturation throughout the diffusion layer, shown in Fig. 3a.

Using the explicit Eq. 44 gives $j_{\lim} \approx 7.3$ A cm^{-2}, which is slightly lower than the numerical value because it was derived for a higher value $n = 4$.

Mass transport losses.—The limiting current densities calculated in the 44 are well above typical desirable current densities so that the associated concentration overpotentials will be small. With $j = 2$ A cm^{-2}, for example, Eq. 34 gives $\eta_c/b = 0.28$ amounting to at most a few tens of millivolts. It has been pointed out previously that modern diffusion layers do not contribute significantly to transport limitations.[35]

For a water electrolyzer concentration overpotentials are negligible, but the lowered saturation at the catalyst layer can incur a wetting or bubble overpotential η_χ according to Eq. 30. With $\tilde{\lambda} = 4$ and $\bar{s} = s_1 = 0.75$ from Fig. 3 this gives $\eta_\chi/b \approx 0.21$.

Design limitations on $\bar{L}$.—Figure 6 shows the saturation s_1 at the DL-CL interface and the effective diffusivity D_{eff} as well as the associated concentration overpotential as a function of the dimensionless diffusion layer thickness $\bar{L}$. For not too low $s \gtrsim 0.6$, we can use Eq. 44 to calculate explicitly what the maximum dimensionless layer thickness $\bar{L} = Lr_{\max}/K$ is to reach a desired limiting current density $j_{\lim}$[g]

$$\bar{L} \approx \frac{J_n}{1.6\lambda}\left(j_{\lim}^{-1/4} - j_{\lim 0}^{-1/4}\right)^4. \qquad [50]$$

With the values from Table I, this gives $\bar{L} \approx 2 \cdot 10^5$ for $\lambda = 4$ and $\bar{L} \approx 7 \cdot 10^5$ for $\lambda = 1.2$. Despite the different value $m = 4$ used to derive Eq. 50 this is in reasonable agreement with the results of Fig. 6.

The value of $\bar{L} \approx 2 \cdot 10^5$ for $\lambda = 4$ corresponds to a very small maximum pore size of $r_{\max} \approx 0.02$ μm for the same thickness, L and is actually not much smaller than the pores of $r_{\max} \approx 0.1$ μm typically used in a microporous layer.[73,92,93] These microporous layers are, however, typically much thinner than the diffusion layers so that their contribution to the mass transport resistance remains limited.

[f] From the appendix on the Stefan Velocity, a better approximation would be to use $\ln\frac{1}{1-0.21} \approx 0.24$ times the molar volume, but in line the with present dilute approximation we use 0.21, instead.

[g] With Eq. 33 we can also solve Eq. 50 explicitly for L, to give

$$L \approx \frac{\frac{J_n K}{1.6\lambda j_{\lim} r_{\max}}}{\left(1 + \left(\frac{J_n K}{1.6\lambda j_{\lim} r_{\max}} \frac{z_w}{FDc_0}\right)^{1/4}\right)^4}.$$

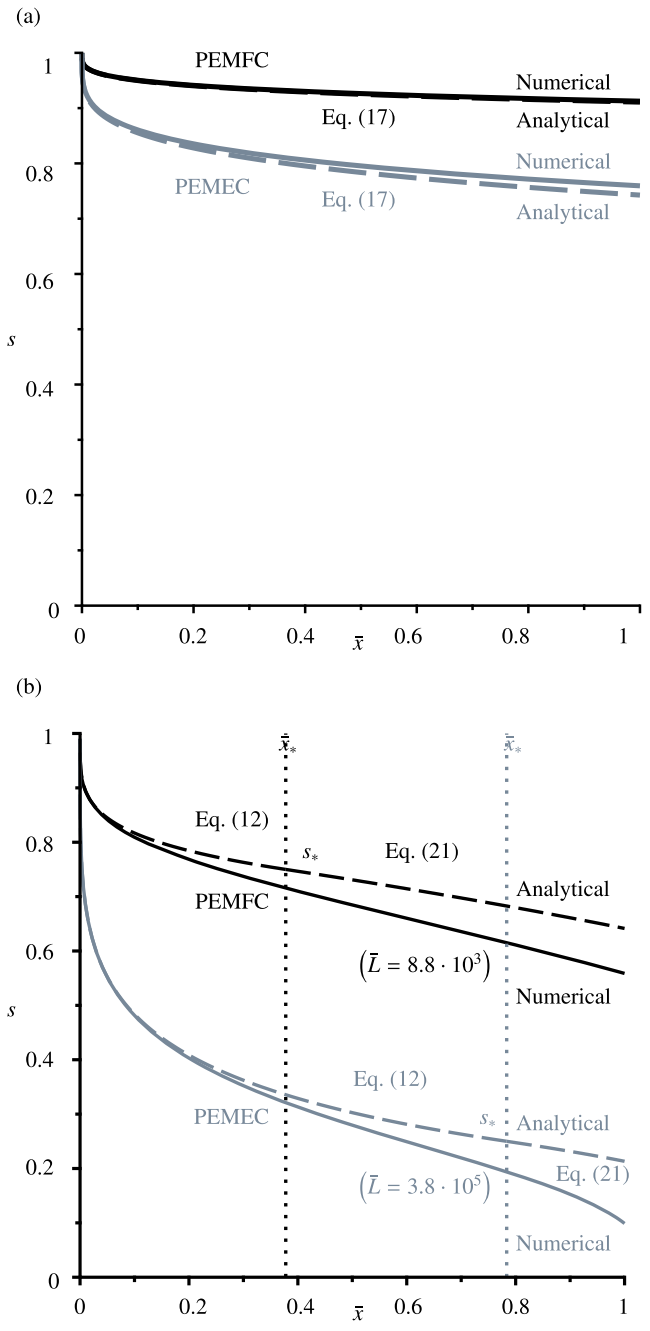

Figure 3. (a) A comparison between the analytical and numerical wetting phase saturation s across the diffusion layer for $j = 2$ A cm^{-2} and the typical diffusion layer properties listed in Table I. For the bottom figure (b) we used a much higher $\bar{L} = 8.8 \cdot 10^3$ and $3.8 \cdot 10^5$ for the PEMFC and PEMWE case respectively to show the effect of, for example, a much smaller pore size. For $\bar{x} < \bar{x}_*$, the non-wetting phase dominates and Eq. 12 is used for analytical solution while for $\bar{x} > \bar{x}_*$, the wetting phase dominates and Eq. 21 is used.

Even for j_{lim}=6 A cm^{-2} the value $\bar{L} = 2 \cdot 10^4$ is well above the 375 in Table I. This shows that even with substantially smaller pores the liquid saturation does not decrease the limiting current density to values in the typically desired operating window. Therefore, the diffusion layer designs are often influenced by other considerations such as electrical resistance and mechanical strength.[94]

When $s_* \gtrsim 0.6$, usually the case for gaseous reactants, we can use Eqs. 25 and 22 to find the value of $\bar{L}$ that corresponds to a desired s_1:

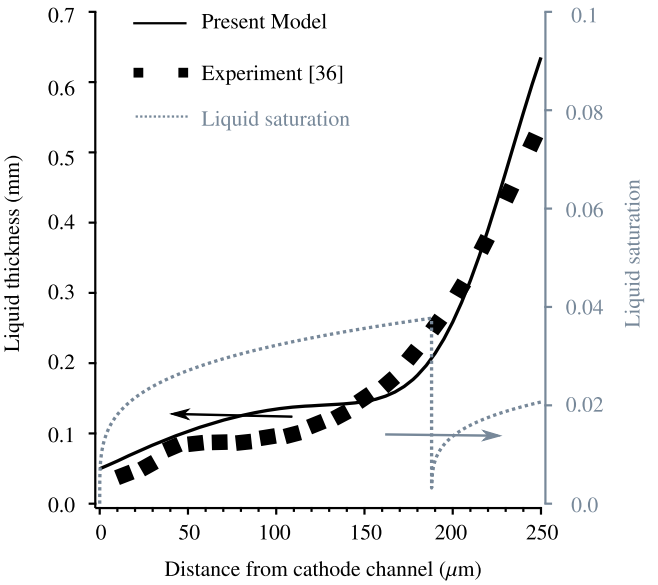

Figure 4. A comparison between liquid thickness obtained using the present analytical model (solid line) and high resolution neutron radiography (black squares) in Ref. 36. The properties of the GDL and the MPL are given in Table II. The analytical saturation profile, shown by dotted line, is obtained by using Eq. 17. It can be seen that there is a significant saturation jump at the GDL-MPL interface due to the smaller pore sizes in the MPL, described by Eq. A·2. The liquid saturation is then converted to liquid thickness using Eq. 49. Due to high water content in the membrane, the neutron radiograph shows higher liquid thickness in the MPL due to scattering of the neutron beam. This scattering effect is applied to the analytical thickness profile using the 1-D Gaussian convolution to give the liquid thickness profile, shown by solid black line. The details of the Gaussian convolution are given in Ref. 36.

$$\bar{L} \approx \begin{cases} \dfrac{J_n}{j_{\max}} \dfrac{(1-s_1)^4}{4\lambda} & s_1 \geqslant s_* \\ \dfrac{J_n}{j_{\max}} \dfrac{(1-s_*)^4}{4\lambda} + \dfrac{J_w}{j_{\max}} \dfrac{s_*^{3-\frac{1}{\lambda}} - s_1^{3-\frac{1}{\lambda}}}{3\lambda - 1} & s_1 < s_*. \end{cases} \quad [51]$$

Using Eq. 9 in the top result gives

$$\frac{(2+\lambda)L}{\alpha \epsilon^3 r_{\max}} \approx \frac{J_n}{j} \left(\frac{1-s_1}{2} \right)^4, \quad s_1 \geqslant s_* \quad [52]$$

where $r_{\max} = 2\gamma|\cos(\theta)|/p_t$ and $J_n = 2\gamma|\cos(\theta)|\, F/V_n\, \mu_n z_n$ from Eqs. 5 and 7. Equation 52 shows the various geometrical diffusion layer parameters on the left, and operational and material parameters on the right.

This shows that, for example, for the same s_1 at a two times higher current density would require, equivalently, halving the DL thickness L, doubling $r_{\max}$ or increasing ϵ by a factor $2^{1/3} \approx 1.26$.

Conclusions

We thoroughly studied the multiphase flow in porous diffusion layers, providing a general unified framework, valid for both PEM or AEM fuel cells and electrolyzers in which the gas and the liquid move in opposite directions. We provide fully analytical expressions that can be readily used to provide guidance on choosing for example the layer thickness and pore size distribution. Such an analytical modeling framework can be useful in understanding the influence of operating and structural parameters on the performance of the diffusion layer and establishes a theoretical understanding of the diffusion layer from relatively general equations.

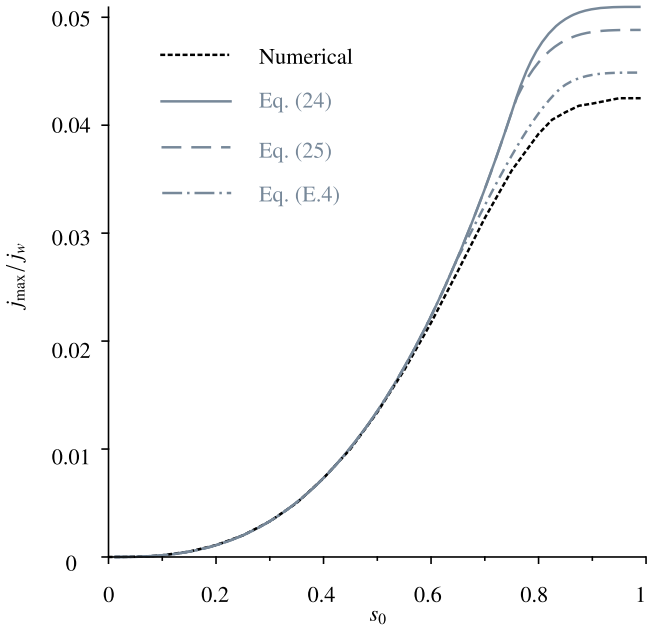

Figure 5. The maximum current for which $s_1 = s_{min} = 0$ as a function of s_0 for the *gaseous* wetting phase properties given in Table I. The solid black line indicates the numerical result obtained by solving Eq. 6, the solid gray line indicates the two-regime 22 and the dashed gray line indicates the three-regime analytical solution described in the appendix on the Three-Regime Solution. In this model we also consider a third domain where the saturation profile is assumed to be linear, and contributions from both $\bar{j}_n$ and $\bar{j}_w$ are important.

We derived accurate semi-analytical expressions for saturation profiles, Eqs. 21 and 17. These were used in Eqs. 22–25 to calculate the maximum current density for which the saturation at the diffusion layer-catalyst layer interface becomes critically low. Equations 44–48 give useful expressions for the diffusion-limited current density.

These results show that for modern gas diffusion layers the wetting phase saturation usually remains above 0.8 so that performance is only modestly impacted and that they are well-designed for their intended operating conditions.

Boundary Condition for s_1

Here we derive what happens when the porosity or wetting properties suddenly change. This is relevant, for example, at the interface between the diffusion layer and microporous layer or catalyst layer, but also at the interface between the diffusion layer and the channel. Neglecting friction over the interface we can use Bernoulli's equation to equate the total pressure $p_i + \frac{1}{2}\rho_i v_i^2$ on either side of the interface. Using a $+$ and $-$ to denote properties right (slightly larger x) and left (lower x) of the interface this gives with $p_c = p_n - p_w$:

$$p_{c-} + \frac{1}{2}(\rho_{n-}v_{n-}^2 - \rho_{w-}v_{w-}^2) = p_{c+} + \frac{1}{2}(\rho_{n+}v_{n+}^2 - \rho_{w+}v_{w+}^2). \quad [A\cdot1]$$

Usually dynamic pressures $\frac{1}{2}\rho_i v_i^2$ are negligible, resulting in the frequently used continuity of capillary pressure $p_{c-} = p_{c+}$.[79,80] With an explicit capillary pressure-saturation relation this can then be used to relate the saturations on either side of the interface. Using e.g. Eq. 4 gives $p_{t-}s_-^{-1/\lambda_-} = p_{t+}s_+^{-1/\lambda_+}$, or

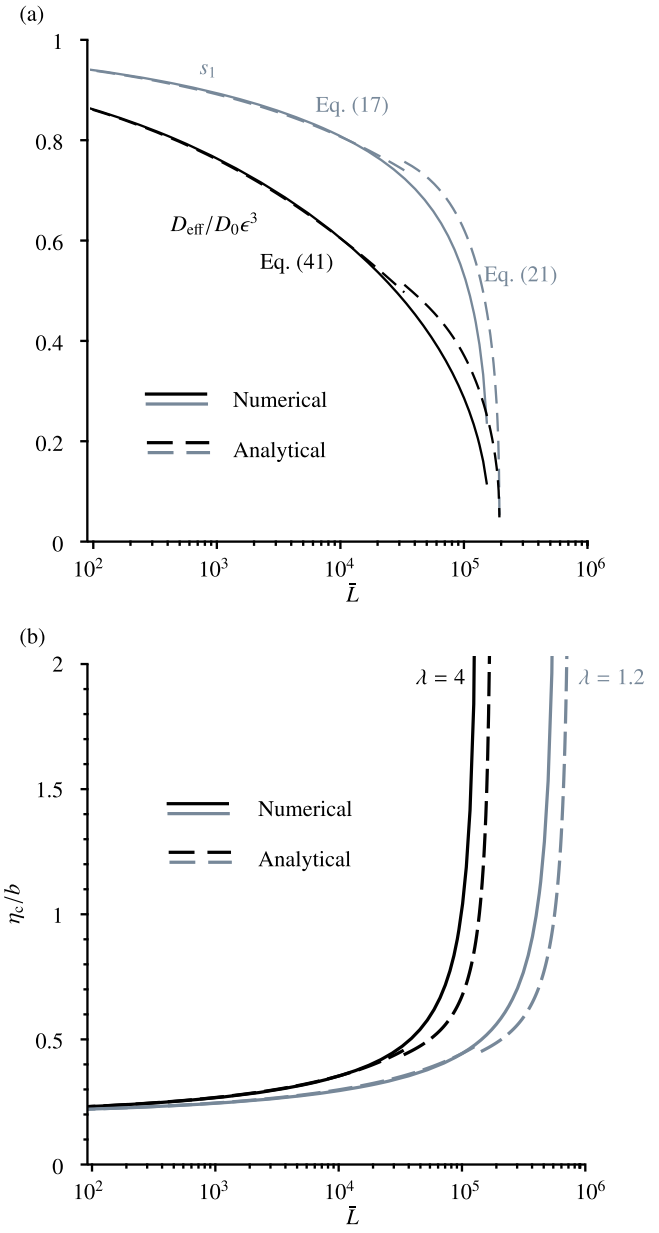

Figure 6. (a) The effective diffusivity D_{eff} (black) and the saturation s_1 (gray) at the DL-CL interface as a function of $\bar{L} = r_{max}L/K$ at a current density of 2 A cm^{-2} for the gaseous wetting phase properties listed in Table I. A discontinuity appears because the approximation Eq. 17 is used only for high s. (b) The associated concentration overpotentials, calculated using Eq. 27. The diffusion coefficient is taken to be equal to $D_{O_2} = 2 \cdot 10^{-5}$ m^2 s^{-1}.

$$s_+ = \left(\frac{p_{t+}}{p_{t-}}\right)^{\lambda_+} s_-^{\lambda_+/\lambda_-}. \quad [A\cdot2]$$

If the threshold pressure of the right medium is much larger than that of the left, as may be the case for a diffusion layer—microporous layer interface this equation may give $s_+ > 1$ so that the dynamic pressure of the non-wetting phase has to be included to give, assuming $\rho_{n+} = \rho_{n-} = \rho_n$

$$\frac{1}{2}\rho_n(v_{n-}^2 - v_{n+}^2)^2 = p_{c+} - p_{c-}. \quad [A\cdot3]$$

The average interstitial velocity $v_n = u_n/\epsilon(1-s)$ where, from Eq. 3 we have $u_n^2 = (z_n V_n j/F)^2$. With an capillary pressure-saturation relation like 4 this gives an explicit relation between s_+ and s_- that has to be solved numerically in general. There are obviously several assumptions in this analysis that require further investigation and validation, which is beyond the scope of this work.

Boundary Condition for s_0

Near $x = 0$, the presence of bubbles or droplets on the diffusion layer surface may cause the saturation to show variations also in the normal directions as schematically indicated in Fig. B·1 similar to what was postulated for near the catalyst layer in Ref. 73. Likely this disturbance from one-dimensional profiles is of the order of the droplets or bubble. Here we will assume the transition zone to be negligibly thin compared to the diffusion layer thickness. The capillary pressure of the droplets or bubbles will be

$$p_{c-} \approx \frac{2\gamma|\cos(\theta)|}{R_c} = p_t \frac{r_{\max}}{R_c}, \qquad [B\cdot1]$$

where R_c is the radius of curvature of the bubble or droplet. Here we assumed that the contact angle is the same as inside the porous medium. Correcting for an effective contact angle will be possible using the Cassie-Baxter equation.[95,96]

Usually $R_c \gg r_{\max}$ so that the capillary pressure of the droplets or bubbles is negligible compared to that inside the porous medium. With $p_{c+} = p_t s_0^{-1/\lambda}$ this implies that s_0 will be close to unity. Neglecting therefore the dynamic pressure of the wetting-phase, we can use Eq. A·3 to write

$$\frac{\rho_n u_n^2}{2p_t}\left(\frac{1}{\Theta^2} - \frac{1}{\epsilon^2(1-s_0)^2}\right)^2 = s_0^{-1/\lambda} - \frac{r_{\max}}{R_c}, \qquad [B\cdot2]$$

where Θ is the fractional bubble coverage, for which correlations exist in terms of j.[97] This implicit relation for s_0 can be re-written to

$$s_0 \approx 1 - \frac{1}{\epsilon\sqrt{\frac{1}{\Theta^2} - \sqrt{\frac{2p_t}{\rho_n u_n^2}\left(s_0^{-1/\lambda} - \frac{r_{\max}}{R_c}\right)}}}, \qquad [B\cdot3]$$

where $u_n^2 = (z_n V_n j/F)^2$. In the unusual circumstance dynamic pressures dominate over capillary pressures this gives for the saturation of the wetting phase $1 - s_0 \approx \Theta/\epsilon$, which represents the fraction of the pores covered with the non-wetting phase. In the more common case of dominant capillary pressure this gives that s_0 is close to unity. With $r_{\max} \ll R_c$ Eq. 10 results.

Stefan Velocity

In the 1 model equations we assume purely convective transport of reactants. However, if the reactant forms only a small fraction of the total wetting phase it will be transported primarily by diffusion, as assumed in the section on 3. Here we consider the general case in which transport consists of both diffusion and advection, a problem referred to as Stefan flow.

Consider the case of a reacting species with concentration c and a non-reacting species with concentration c_N. The may, for example, correspond to oxygen and nitrogen in an air mixture at the cathode of a fuel cell. We assume that the total concentration

$$C = c_N + c \qquad [C\cdot1]$$

is a constant, which is a good approximation for gases. The flux of non-reacting species $uc_N - Ddc_N/dx = 0$, with D the mutual diffusion coefficient. Or, with Eq. C·1:

$$0 = u(C-c) + D\frac{dc}{dx}. \qquad [C\cdot2]$$

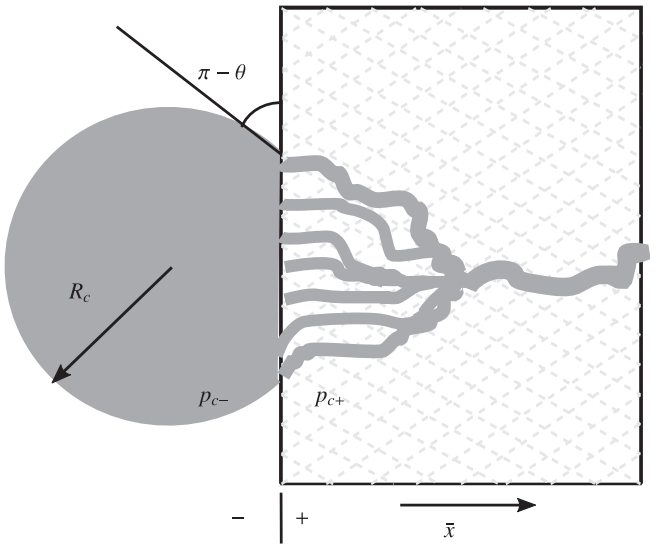

Figure B·1. Schematic of a potential transition region near a droplet (or bubble, in which case $\pi - \theta$ becomes θ) the flow channel, we assume any deviation from one-dimensionality to be negligible. The "-" and "+" are denoted in the figure. The contact angle is denoted as θ and the radius of curvature of bubble/droplet is denoted as R_c.

With boundary conditions $c_0 = fC$ at the flow channel at $x = 0$ and $c_1 = 0$ at the CL at $x = L$, the differential Eq. C·2 can be solved for the Stefan velocity u as

$$u = \frac{D}{L}\ln\frac{1}{1-f}. \qquad [C\cdot3]$$

Using Eq. C·2, the reacting species flux is $N = uc - Ddc/dx = uC$ so that the velocity reads $u = N/C = fN/c_0$. We thus see that in Eq. 3 the molar volume is that of the total mixture. In the dilute limit $f \ll 1$ we have $\ln\frac{1}{1-f} \approx f$ so that from Eq. C·3 Fick's law $N = uC = \frac{Dc_0}{L}$ is obtained.

Udell Leverett-J Function

The dimensionless capillary pressure p_c/p_t is often referred to as the Leverett J-function. In the main text we used $J(s) = s^{-\lambda}$. A particularly popular function is that by Udell:[33]

$$J(s) = 1.417(1-s) - 2.12(1-s)^2 + 1.263(1-s)^3. \qquad [D\cdot1]$$

Note that in Eq. D·1 the capillary pressure vanishes for $s = 1$, the pressure p_t is no longer associated with the capillary pressure of the largest pores as in Eq. 5. Equation 6 is now replaced by

$$\frac{dJ(s)}{ds}\frac{ds}{d\bar{x}} = \frac{\bar{j}_n}{(1-s)^3} + \frac{\bar{j}_w}{s^3}, \qquad [D\cdot2]$$

Similar to the main text we can again introduce a non-wetting phase integral

$$I_n \equiv \int_0^s (1-s)^3 \frac{dJ(s)}{ds} ds = (1-s)^4\left(\frac{1.417}{4} - \frac{4.24(1-s)}{5} + \frac{3.789(1-s)^2}{6}\right) - 0.13775 \qquad [D\cdot3]$$

Note that Eq. D·1 corresponds to a fixed normalized pore size distribution, so there is no free parameter like λ in the Brooks-Corey model. The slope $\frac{1}{p_t}\frac{dp_c}{ds}\Big|_{s=1} = -1.417$ using Eq. D·1. This is equal to

the $-1/\lambda$ of the Brooks-Corey model. The variation in capillary pressure however is much smaller for intermediate s. At $s = 0.5$, for example, the same slope is obtained for $\lambda \approx 9$. For s close to 1, solving $-1.417\frac{ds}{d\bar{x}} = \frac{\bar{j}_n}{(1-s)^3}$, similar to Eq. 15, gives

$$s \approx 1 - (2.82\bar{j}_n\,\bar{x})^{1/4}. \qquad [D{\cdot}4]$$

Similarly, for $I_w(s)$, we have

$$\begin{aligned} I_w &\equiv \int_0^s s^3 \frac{dJ(s)}{ds} ds \\ &= -s^4(0.6315s^2 - 0.6676s + 0.2415) \end{aligned} \qquad [D{\cdot}5]$$

The integrals Eqs. D·3 and D·5 can be used in, for example, Eqs. 12, 12, and 41 to calculate for example $j_{\max}$ and $j_{\lim}$.

Three-regime Solution

In the analysis of the main text, we always neglect one of the pressure gradients in Eq. 6. However, around s_*, both the wetting phase and the non-wetting phase pressure gradients are important. We define $s_{*,1}$ as the saturation above which the ratio $\frac{dp_n/dx}{dp_w/dx} = \frac{k_w j_w}{k_n j_n} \gtrsim 5$ and we neglect the wetting phase pressure gradient. We also define $s_{*,2}$ as the saturation below which the ratio $\frac{dp_w/dx}{dp_n/dx} = \frac{k_n j_n}{k_w j_w} \gtrsim 5$ and we neglect the non-wetting phase pressure gradient.[h]

By using Eq. 6 and above definition for $s_{*,1}$ and $s_{*,2}$, we can write

$$s_{*,1} = \frac{1}{1 + \left(\frac{j_w}{5j_n}\right)^{1/3}}, \quad \text{and} \quad s_{*,2} = \frac{1}{1 + \left(\frac{j_w}{5j_n}\right)^{1/3}}. \qquad [E{\cdot}1]$$

When $s > s_{*,1}$, we use Eq. 12 to calculate the saturation. When $s < s_{*,2}$, we use Eq. 21 to calculate the saturation. For $s_{*,1} < s < s_{*,2}$, we consider a linear variation of saturation. At $s_a \equiv (s_{*,1} + s_{*,2})/2$, using Eq. 6 we can write

$$\left.\frac{ds}{d\bar{x}}\right|_{\bar{x}=\bar{x}_a} = \left(\frac{\bar{j}_n}{(1-s_a)^3} - \frac{\bar{j}_w}{s_a^3}\right)\lambda s_a^{\frac{1}{\lambda}+1}. \qquad [E{\cdot}2]$$

The non-dimensional coordinates $\bar{x}_{*,1}$ at which $s = s_{*,1}$ and $\bar{x}_{*,2}$ at which $s = s_{*,2}$ are evaluated using Eq. 12 or Eq. 13. If $s_{*,2} < s_0 < s_{*,1}$, we take $\bar{x}_{*,1} = 0$ and $s_{*,1} = s_0$ in Eq. E·2. In the linear part, we then have

$$s = s_{*,1} + (\bar{x} - \bar{x}_{*,1})\left.\frac{ds}{d\bar{x}}\right|_{\bar{x}=\bar{x}_a}. \qquad [E{\cdot}3]$$

The limiting current for a three-regime analysis is given as

$$\frac{j_{\max}}{j_w} = \frac{s_{*,2}^{\frac{3\lambda-1}{\lambda}} - s_{\min}^{\frac{3\lambda-1}{\lambda}}}{(1-\bar{x}_{*,2})(3\lambda-1)}. \qquad [E{\cdot}4]$$

ORCID

A. Rajora https://orcid.org/0000-0002-9942-5353
J. W. Haverkort https://orcid.org/0000-0001-5028-5292

References

1. J. D. Fonseca, M. Camargo, J.-M. Commenge, L. Falk, and I. D. Gil, *Int. J. Hydrogen Energy*, **44**, 9486 (2019).
2. A. Scipioni, A. Manzardo, and J. Ren, *Hydrogen Economy: Supply Chain, Life Cycle Analysis and Energy Transition for Sustainability* (Academic Press, Elsevier, New York) (2017), www.sciencedirect.com/book/9780128111321/hydrogen-economy.
3. T. Wilberforce, Z. El-Hassan, F. Khatib, A. Al Makky, A. Baroutaji, J. G. Carton, J. Thompson, and A. G. Olabi, *Int. J. Hydrogen Energy*, **42**, 25639 (2017).
4. J. Shin, W.-S. Hwang, and H. Choi, *Technol. Forecast. Soc. Change*, **143**, 239 (2019).
5. P. Tiwari, G. Tsekouras, K. Wagner, G. F. Swiegers, and G. G. Wallace, *Int. J. Hydrogen Energy*, **44**, 23568 (2019).
6. D. L. Fritz, J. Mergel, and D. Stolten, *ECS Trans.*, **58**, 1 (2014).
7. E. T. Ojong, J. T. H. Kwan, A. Nouri-Khorasani, A. Bonakdarpour, D. P. Wilkinson, and T. Smolinka, *Int. J. Hydrogen Energy*, **42**, 25831 (2017).
8. C. H. Lee, R. Banerjee, F. Arbabi, J. Hinebaugh, and A. Bazylak, *VIII Int. Conf. Nanochannels, Microchannels, Minichannels***50343**, V001T07A003 (2016).
9. M. Zlobinski, T. Schuler, F. N. Büchi, T. J. Schmidt, and P. Boillat, *J. Electrochem. Soc.*, **167**, 084509 (2020).
10. J. Garcia-Navarro, M. Schulze, and K. A. Friedrich, *ACS Sustainable Chem. Eng.*, **7**, 1600 (2018).
11. P. Trinke, G. Keeley, M. Carmo, B. Bensmann, and R. Hanke-Rauschenbach, *J. Electrochem. Soc.*, **166**, F465 (2019).
12. B. Braz, V. Oliveira, and A. Pinto, *Int. J. Hydrogen Energy*, **44**, 19334-19343 (2019).
13. G. Zhang and K. Jiao, *J. Power Sources*, **391**, 120 (2018).
14. X. Liu, F. Peng, G. Lou, and Z. Wen, *J. Power Sources*, **299**, 85 (2015).
15. A. H. A. Rahim, A. S. Tijani, S. K. Kamarudin, and S. Hanapi, *J. Power Sources*, **309**, 56 (2016).
16. A. Zinser, G. Papakonstantinou, and K. Sundmacher, *Int. J. Hydrogen Energy*, **44**, 28077 (2019).
17. G. Schmidt, M. Suermann, B. Bensmann, R. Hanke-Rauschenbach, and I. Neuweiler, *J. Electrochem. Soc.*, **167**, 114511 (2020).
18. T. E. Lipman and A. Z. Weber, *Fuel Cells And Hydrogen Production: A Volume in the Encyclopedia of Sustainability Science and Technology* (Springer, Berlin) (2019).
19. A. Z. Weber and J. Newman, *J. Electrochem. Soc.*, **152**, A677 (2005).
20. A. G. Stern, *Int. J. Hydrogen Energy*, **43**, 4244 (2018).
21. T. Shinagawa and K. Takanabe, *ChemSusChem*, **10**, 1318 (2017).
22. T. J. Jacobsson, V. Fjällström, M. Edoff, and T. Edvinsson, *Energy Environ. Sci.*, **7**, 2056 (2014).
23. H. R. Corti and E. R. Gonzalez, *Direct Alcohol Fuel Cells* (Springer, Berlin) 1 (2014).
24. G. Deng, L. Liang, C. Li, J. Ge, C. Liu, Z. Jin, and W. Xing, *J. Power Sources*, **427**, 120 (2019).
25. P. Joghee, J. N. Malik, S. Pylypenko, and R. O'Hayre, *MRS Energy Sustain*, **2**, E3 (2015).
26. W. Yang, M. Lu, and Y. He, *Int. J. Hydrogen Energy*, **41**, 20693 (2016).
27. S. Badwal, S. Giddey, A. Kulkarni, J. Goel, and S. Basu, *Appl. Energy*, **145**, 80 (2015).
28. S. Huo and K. Jiao, *Anion Exchange Membrane Fuel Cells* (Springer, Berlin) 169-215 (2018).
29. F. Kubannek, T. Turek, and U. Krewer, *Chem. Ing. Tech.*, **91**, 720 (2019).
30. B. De Mot, J. Hereijgers, M. Duarte, and T. Breugelmans, *Chem. Eng. J.*, **378**, 122224 (2019).
31. L.-C. Weng, A. T. Bell, and A. Z. Weber, *Phys. Chem. Chem. Phys.*, **20**, 16973 (2018).
32. T. Burdyny and W. A. Smith, *Energy Environ. Sci.*, **12**, 1442 (2019).
33. U. Pasaogullari and C.-Y. Wang, *Electrochim. Acta*, **49**, 4359 (2004).
34. J. H. Nam and M. Kaviany, *Int. J. Heat Mass Transfer*, **46**, 4595 (2003).
35. A. Z. Weber, *J. Power Sources*, **195**, 5292 (2010).
36. J. S. Preston, R. S. Fu, U. Pasaogullari, D. S. Hussey, and D. L. Jacobson, *J. Electrochem. Soc.*, **158**, B239 (2010).
37. A. Bazylak, *International journal of hydrogen energy*, **34**, 3845 (2009).
38. S. Park, J.-W. Lee, and B. N. Popov, *Journal of Power Sources*, **177**, 457 (2008).
39. D. Muirhead, R. Banerjee, M. G. George, N. Ge, P. Shrestha, H. Liu, J. Lee, and A. Bazylak, *Electrochimica Acta*, **274**, 250 (2018).
40. S. Grigoriev, A. Kalinnikov, P. Millet, V. Porembsky, and V. Fateev, *J. Appl. Electrochem.*, **40**, 921 (2010).
41. J. Hu, J. Li, L. Xu, F. Huang, and M. Ouyang, *Energy*, **111**, 869 (2016).
42. D. Natarajan and T. Van Nguyen, *Journal of Power Sources*, **115**, 66 (2003).
43. S. Litster and N. Djilali, *Transport Phenomena in Fuel Cells* (WIT Press, Southampton) 19, p. 175 (2005).
44. Y.-S. Wu, *Multiphase Fluid Flow in Porous and Fractured Reservoirs* (Gulf Professional Publishing, Massachusetts) (2015).
45. G. F. Pinder and W. G. Gray, *Essentials of Multiphase Flow and Transport in Porous Media* (John Wiley & Sons, New Jersey) (2008).
46. S. Huo, K. Jiao, and J. W. Park, *Appl. Energy*, **233**, 776 (2019).
47. M. T. Van Genuchten, *Soil Sci. Soc. Am. J.*, **44**, 892 (1980).
48. R. H. Brooks and A. T. Corey, "Hydraulic properties of porous media." *Hydrology Papers* (Colorado State University, Colorado)3 (1964).
49. B. Xiao, W. Wang, X. Zhang, G. Long, H. Chen, H. Cai, and L. Deng, *Fractals*, **27**, 1950012 (2019).
50. Y. Shi, S. Cheng, and S. Quan, *J. Power Sources*, **209**, 130 (2012).
51. J. Kim, G. Luo, and C.-Y. Wang, *J. Power Sources*, **400**, 284 (2018).
52. V. Gurau and J. A. Mann Jr, *J. Electrochem. Soc.*, **157**, B512 (2010).
53. J. Roth, "Water transport in gas diffusion media for PEM fuel cells: experimental and numerical investigation." *Ph.D. Thesis*, Duisburg-Essen University (2010).
54. L. Zhu, J. Xu, Y. Xiu, Y. Sun, D. W. Hess, and C.-P. Wong, *The Journal of Physical Chemistry B*, **110**, 15945 (2006).

[h] We chose the ratio $\frac{dp_n/dx}{dp_w/dx} \gtrsim 5$ to neglect dp_w/dx and $\frac{dp_w/dx}{dp_n/dx} \gtrsim 5$ to neglect dp_n/dx as it gives the best approximation for the numerical solution. For values between 3 and 8, the analytical solution does not change significantly but for higher or lower values, the analytical solution gives a larger deviation.

55. P. Satjaritanun and I. V. Zenyuk, *Current Opinion in Electrochemistry* (2020).
56. W. Cui, H. Ma, B. Tian, Y. Ji, and F. Su, *J. Mater. Sci.*, **51**, 4031 (2016).
57. V. Peykov, A. Quinn, and J. Ralston, *Colloid and Polymer Science*, **278**, 789 (2000).
58. D. Fernandez, P. Maurer, M. Martine, J. Coey, and M. E. Mobius, *Langmuir*, **30**, 13065 (2014).
59. K. Nakornthap and R. D. Evans et al., *SPE Reservoir Eng.*, **1**, 230 (1986).
60. H. Rajaei, A. Rajora, and J. W. Haverkort, *Journal of Power Sources*, **491**, 229364 (2021).
61. Y. Cengel, *Heat and Mass Transfer: Fundamentals and Applications* (McGraw-Hill Higher Education, New York) (2014).
62. W. G. Bessler, *J. Electrochem. Soc.*, **153**, A1492 (2006).
63. N. W. Lee, Y. S. Kim, M. Kim, and M. S. Kim, *J. Mech Sci. Technol.*, **30**, 4383 (2016).
64. T. V. Nguyen and R. E. White, *J. Electrochem. Soc.*, **140**, 2178 (1993).
65. A. Rowe and X. Li, *Journal of Power Sources*, **102**, 82 (2001).
66. M. Wyllie and M. Spangler, *AAPG Bulletin*, **36**, 359-403 (1952).
67. C. C. Huet, "Semi-analytical estimates of permeability obtained from capillary pressure." *Ph.D. Thesis*, Texas A&M University (2006).
68. J. Kozeny, *Royal Academy of Science, Vienna, Proc. Class I*, **136**, 271-306 (1927).
69. D. Muirhead, R. Banerjee, M. G. George, N. Ge, P. Shrestha, H. Liu, J. Lee, and A. Bazylak, *Electrochim. Acta*, **274**, 250 (2018).
70. L. An, T. Zhao, Z. Chai, P. Tan, and L. Zeng, *Int. J. Hydrogen Energy*, **39**, 19869 (2014).
71. B. Han, J. Mo, Z. Kang, G. Yang, W. Barnhill, and F.-Y. Zhang, *Int. J. Hydrogen Energy*, **42**, 4478 (2017).
72. X. Wang and T. Van Nguyen, *J. Electrochem. Soc.*, **155**, B1085 (2008).
73. J. H. Nam, K.-J. Lee, G.-S. Hwang, C.-J. Kim, and M. Kaviany, *Int. J. Heat Mass Transfer*, **52**, 2779 (2009).
74. J. W. Haverkort, *Electrochim. Acta*, **295**, 846 (2019).
75. J. Herranz, J. Durst, E. Fabbri, A. Patru, X. Cheng, A. A. Permyakova, and T. J. Schmidt, *Nano Energy*, **29**, 4 (2016).
76. F. Marangio, M. Santarelli, and M. Cali, *Int. J. Hydrogen Energy*, **34**, 1143 (2009).
77. Z. Kang, S. M. Alia, J. L. Young, and G. Bender, *Electrochim. Acta*, **354**, 136641 (2020).
78. Y. M. Volfkovich, E. Shkolnikov, V. Dubasova, and V. Ponomarev, *Sov. Electrochem*, **19**, 681-688 (1983).
79. F. Ahmadi and R. Roshandel, *J. Fuel Cell Sci. Technol.*, **11**, 011004 (2014).
80. R. Wu, Q. Liao, X. Zhu, and H. Wang, *Int. J. Heat Mass Transfer*, **55**, 6363 (2012).
81. A. Z. Weber and J. Newman, *Chem. Rev.*, **104**, 4679 (2004).
82. Y. Wang and S. Wang, *Int. J. Heat Mass Transfer*, **105**, 18 (2017).
83. G. Hwang and A. Weber, *J. Electrochem. Soc.*, **159**, F683 (2012).
84. Y. Wang, S. Wang, S. Liu, H. Li, and K. Zhu, *Electrochimica Acta*, **318**, 770 (2019).
85. T. G. Tranter, P. Boillat, A. Mularczyk, V. Manzi-Orezzoli, P. R. Shearing, D. Brett, J. Eller, J. Gostick, and A. Forner-Cuenca, *J. Electrochem. Soc.*, **167**, 114512 (2020).
86. J. T. Gostick, M. W. Fowler, M. A. Ioannidis, M. D. Pritzker, Y. M. Volfkovich, and A. Sakars, *J. Power Sources*, **156**, 375 (2006).
87. A. El-Kharouf, T. J. Mason, D. J. Brett, and B. G. Pollet, *J. Power Sources*, **218**, 393 (2012).
88. S. Grigoriev, P. Millet, S. Volobuev, and V. Fateev, *Int. J. Hydrogen Energy*, **34**, 4968 (2009).
89. J. T. Gostick, M. W. Fowler, M. D. Pritzker, M. A. Ioannidis, and L. M. Behra, *Journal of Power Sources*, **162**, 228 (2006).
90. R. Lenhard, J. Parker, and S. Mishra, *Journal of Irrigation and Drainage Engineering*, **115**, 744 (1989).
91. J. Ihonen, M. Mikkola, and G. Lindbergh, *J. Electrochem. Soc.*, **151**, A1152 (2004).
92. J. Becker, C. Wieser, S. Fell, and K. Steiner, *Int. J. Heat Mass Transfer*, **54**, 1360 (2011).
93. X. Zhang, Y. Gao, H. Ostadi, K. Jiang, and R. Chen, *Int. J. Hydrogen Energy*, **39**, 17222 (2014).
94. D. Qiu, H. Janßen, L. Peng, P. Irmscher, X. Lai, and W. Lehnert, *Appl. Energy*, **231**, 127 (2018).
95. A. Cassie and S. Baxter, *Trans. Faraday Soc.*, **40**, 546 (1944).
96. J. Z. Fishman, H. Leung, and A. Bazylak, *Int. J. Hydrogen Energy*, **35**, 9144 (2010).
97. H. Vogt, *Electrochim. Acta*, **78**, 183 (2012).